

Article

Low Subthreshold Slope AlGa_N/Ga_N MOS-HEMT with Spike-Annealed HfO₂ Gate Dielectric

Min Jae Yeom¹, Jeong Yong Yang¹ , Chan Ho Lee¹, Junseok Heo² , Roy Byung Kyu Chung^{3,*} 
and Geonwook Yoo^{1,*} 

¹ School of Electronic Engineering, Soongsil University, Seoul 06938, Korea; duaalswo94@gmail.com (M.J.Y.); skholda94@gmail.com (J.Y.Y.); yahco61@gmail.com (C.H.L.)

² Department of Electrical and Computer Engineering, Ajou University, Suwon 16499, Korea; jsseo@ajou.ac.kr

³ Department of Electronic Materials Science and Engineering, Kyungpook National University, Daegu 41566, Korea

* Correspondence: roy.b.chung@knu.ac.kr (R.B.K.C.); gwyoo@ssu.ac.kr (G.Y.)

Abstract: AlGa_N/Ga_N metal-oxide semiconductor high electron mobility transistors (MOS-HEMTs) with undoped ferroelectric HfO₂ have been investigated. Annealing is often a critical step for improving the quality of as-deposited amorphous gate oxides. Thermal treatment of HfO₂ gate dielectric, however, is known to degrade the oxide/nitride interface due to the formation of Ga-containing oxide. In this work, the undoped HfO₂ gate dielectric was spike-annealed at 600 °C after the film was deposited by atomic layer deposition to improve the ferroelectricity without degrading the interface. As a result, the subthreshold slope of AlGa_N/Ga_N MOS-HEMTs close to 60 mV/dec and on/off ratio > 10⁹ were achieved. These results suggest optimizing the HfO₂/nitride interface can be a critical step towards a low-loss high-power switching device.

Keywords: MOS-HEMT; ALD HfO₂; Spike annealing; ferroelectric



Citation: Yeom, M.J.; Yang, J.Y.; Lee, C.H.; Heo, J.; Chung, R.B.K.; Yoo, G.

Low Subthreshold Slope AlGa_N/Ga_N MOS-HEMT with Spike-Annealed HfO₂ Gate Dielectric. *Micromachines* **2021**, *12*, 1441.

<https://doi.org/10.3390/mi12121441>

Academic Editor: Benoit Bakeroot

Received: 13 October 2021

Accepted: 23 November 2021

Published: 25 November 2021

Publisher's Note: MDPI stays neutral with regard to jurisdictional claims in published maps and institutional affiliations.



Copyright: © 2021 by the authors. Licensee MDPI, Basel, Switzerland. This article is an open access article distributed under the terms and conditions of the Creative Commons Attribution (CC BY) license (<https://creativecommons.org/licenses/by/4.0/>).

1. Introduction

III-Nitrides (InN, GaN, and AlN) are well-known for their intrinsic spontaneous polarization and piezo-electricity. Furthermore, AlN and GaN exhibit large bandgap energy of 6.2 and 3.4 eV, respectively. Owing to these excellent material properties, AlGa_N/Ga_N-based HEMTs have been extensively studied and are being commercialized for high-frequency and high-power applications [1–3]. Along with the vast improvement of material quality of nitrides, there have been significant improvements in device design to enhance the performance and reliability of HEMTs throughout the years [4,5]. To reduce the gate leakage and drain current collapse, for example, MOS-HEMTs have been developed with various high-k dielectrics such as Al₂O₃, Y₂O₃, and HfO₂ [6–8]. HfO₂ is a very promising gate dielectric for HEMTs due to its large bandgap (5.3–5.8 eV) and high dielectric constant (20–25).

HfO₂ is especially interesting as a gate dielectric because of its ferroelectricity [9]. Ferroelectric gate can lead to a host of new and novel devices such as nonvolatile memory, radio-frequency, and neuromorphic devices [10,11]. When combined with AlGa_N/Ga_N HEMTs, the reconfigurable polarization of HfO₂ means polarization engineering for 2-dimensional electron gas (2DEG) channel. One of the advantages of polarization engineering is the ability to modulate the carrier density of 2DEG to lower the subthreshold slope (SS) and therefore reduce switching power loss. A large threshold voltage tuning (range: 2.8 V) and reduction of SS have been demonstrated with Hf_{0.5}Zr_{0.5}O₂-based ferroelectric gate HEMTs recently [12]. While very promising, the effectiveness of a HfO₂-based ferroelectric gate for HEMTs remains somewhat elusive as the reported average values of SS were still relatively large (160–180 mV/dec). Furthermore, it has been reported the interface of HfO₂/Ga_N prone to the formation of unfavorable Ga–O bonds, which could potentially become interfacial traps [13].

In this work, AlGaIn/GaN-based MOS-HEMTs with SS near 60 mV/dec and an on/off ratio of $>10^9$ have been demonstrated. Undoped HfO_2 was deposited by ALD as a gate dielectric. After spike-annealing, the ferroelectric property of HfO_2 was assessed via high-resolution transmission electron microscopy (HR-TEM) and polarization voltage (P-V) PUND (Positive Up Negative Down) measurements on the fabricated $\text{HfO}_2/\text{AlGaIn}$ MOSCAP. Due to the atomically abrupt $\text{HfO}_2/\text{nitride}$ interface and the spike annealing-induced orthorhombic phase in HfO_2 film, the counterclockwise ferroelectric hysteresis was observed. As a result, a low SS value near 60 mV/dec could be achieved without compromising the overall performance of AlGaIn/GaN MOS-HEMTs.

2. Experimental

Figure 1a shows the cross-sectional schematic of fabricated MOS-HEMTs with HfO_2 gate dielectric. The AlGaIn/GaN structure was grown by metal–organic chemical vapor deposition on a sapphire substrate, consisting of a 50-nm GaN nucleation layer, a 2 μm semi-insulating GaN:Fe buffer, a 50 nm undoped GaN channel, 1 nm AlN interlayer, a 25 nm $\text{Al}_{0.25}\text{Ga}_{0.75}\text{N}$ barrier, and a 3 nm GaN capping layer. The room-temperature Hall mobility and sheet carrier concentration were $2200 \text{ cm}^2/\text{Vs}$ and $7.9 \times 10^{12} \text{ cm}^{-2}$, respectively. After cleaning the sample using acetone and 2-isopropanol (IPA) for 10 min each in an ultrasonicator, a 30 nm thick ($1\text{\AA}/\text{cycle}$) HfO_2 dielectric layer was deposited by atomic layer deposition (ALD) at the stage temperature of 350°C . For the ALD process of HfO_2 , tetrakis (ethylmethylamino) hafnium (TEMAH) was the precursor and ozone was the reactant. A mesa was formed using Cl_2/BCl_3 inductively-coupled plasma reactive ion etcher. After the mesa formation, a Ti/Al (75/180nm) stack was deposited by and an e-beam evaporator for the ohmic source (S) and drain (D) contacts. These contacts and the gate oxide were spike-annealed at 600°C for 90 sec and 900°C for 30 sec using a rapid thermal annealing (RTA) process in the N_2 atmosphere [14]. The ramp-up rates were $30^\circ\text{C}/\text{sec}$ from room temperature to 600°C and $90^\circ\text{C}/\text{sec}$ from 600 to 900°C . The cooling rate was $150^\circ\text{C}/\text{min}$. The purpose of the first annealing step is twofold. While it is a temperature stabilization step before a spike annealing step, it is also to improve the ohmic contact and induce a phase transition within HfO_2 for ferroelectricity. The second annealing step is solely to lower the contact resistance. The annealing had to be shortened to protect the ferroelectric phase in HfO_2 and maintain the abrupt interface. As a result, the temperature had to be raised above normal ohmic contact annealing temperature (850°C). To minimize the gate leakage through the grain boundary between the crystallized HfO_2 , a 30 nm thick amorphous HfO_2 dielectric layer was deposited under the same ALD condition [15,16]. Finally, Ni/Au (20/50 nm) contact was formed on the gate dielectric. Figure 1b shows summarized process steps.

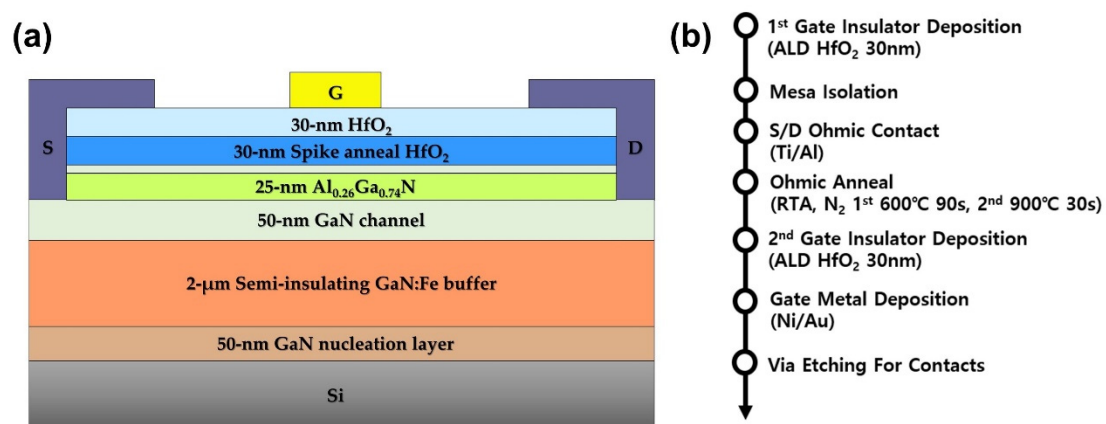


Figure 1. (a) A cross-sectional schematic of fabricated MOS-HEMTs with spike RTA HfO_2 gate dielectric. (b) Summarized process steps.

The electrical performance of fabricated MOS-HEMT was conducted via DC and PUND measurement. A 4200A-SCS semiconductor parameter analyzer (Solon, OH, USA) was used for I-V measurements. PMU-4225 (Solon, OH, USA) with a remote pulse measure unit is used to perform PUND measurements. Additional source meter and DC power supply (Keithley 2410 and 2220G, Solon, OH, USA) were set up to apply a high voltage and measure breakdown voltage. The structural and interfacial analyses of the oxide-semiconductor structure were performed using TEM.

3. Results and Discussion

It has been reported that HfO₂ can be ferroelectric when doped with elements including Al, Gd, Si, Zr, etc. [17]. The origin of ferroelectricity in the doped HfO₂ film has been associated with a non-centrosymmetric orthorhombic phase (Pca2₁) [18]. Undoped HfO₂ can also display ferroelectric characteristics when an orthorhombic phase is present [19]. Therefore, regardless of doping, the key to the ferroelectric behavior of HfO₂ is strongly related to an orthorhombic phase within the matrix. Figure 2 shows the cross-sectional TEM image of HfO₂ on AlGa_{0.5}N after the second annealing at 900 °C for 30 sec. Given that the phase transition of HfO₂ starts at ~500 °C [19], the orthorhombic HfO₂ was likely formed during the fast short annealing step at 600 °C. While undesirable for the HfO₂ layer, a 900 °C annealing step is necessary for the ohmic contacts. According to the cross-sectional TEM image, there was no evidence that the second contact annealing degraded the HfO₂/AlGa_{0.5}N interface. The atomically abrupt interface between HfO₂ and AlGa_{0.5}N was observed as indicated by the white dotted box in Figure 2a. The diffraction patterns (zone axis = [100]) from regions 1 and 2 are shown in Figure 2b,c, respectively. Based on the comparison between the measured and simulated patterns (the insets in Figure 2b,c), one can see regions 1 and 2 correspond to the orthorhombic (space group: Pca2₁) and tetragonal (space group: P42/nmc) phase, respectively. In the case of region 2, however, note that the diffraction pattern is a mixture of both phases. This non-centrosymmetric orthorhombic phase within the HfO₂ film is likely the origin of the gate voltage-dependent polarization switching shown in Figure 3. Note that the polarization charge measured from our samples is relatively low in comparison with an undoped HfO₂ layer sandwiched in between TiN. This is likely because of the absence of a capping layer that suppresses the phase transition from the ferroelectric to paraelectric phase [20]. Although the ferroelectric phase and the abrupt HfO₂/AlGa_{0.5}N interface were confirmed by TEM, the 2-step annealing process without a capping layer likely weakened the ferroelectric strength. Details of the ferroelectric property are discussed below.

Due to the unconventional S/D metal scheme adopted in our device structure, transfer length method (TLM) measurements were conducted to characterize the contact resistance of the S/D metal scheme in our device structure [21]. The total resistance (R) for variable gap spacings from 20 μm to 100 μm was calculated from the I_{DS} vs. V_{DS} curves in Figure 4a. After the measured R over the gap spacing is plotted, the contact resistance (R_c) and specific contact resistivity (ρ_c) were extracted as 19.1 Ω·mm and 1.8 × 10⁻³ Ω·cm², respectively through a linear fit on the results as shown in Figure 4b. The relatively high contact resistance is attributed to the contact structure, which is contacted to the 2DEG through the corner of the sidewall, not through AlGa_{0.5}N/GaN layer. However, the sheet resistance (R_{sh}) is extracted as 374 ohm/□, which is close to the sheet resistance measured by the Van der Pauw method. Therefore, the relatively high contact resistance does not seem to interfere with the ferroelectric effect of the spike-annealed HfO₂ layer on 2DEG.

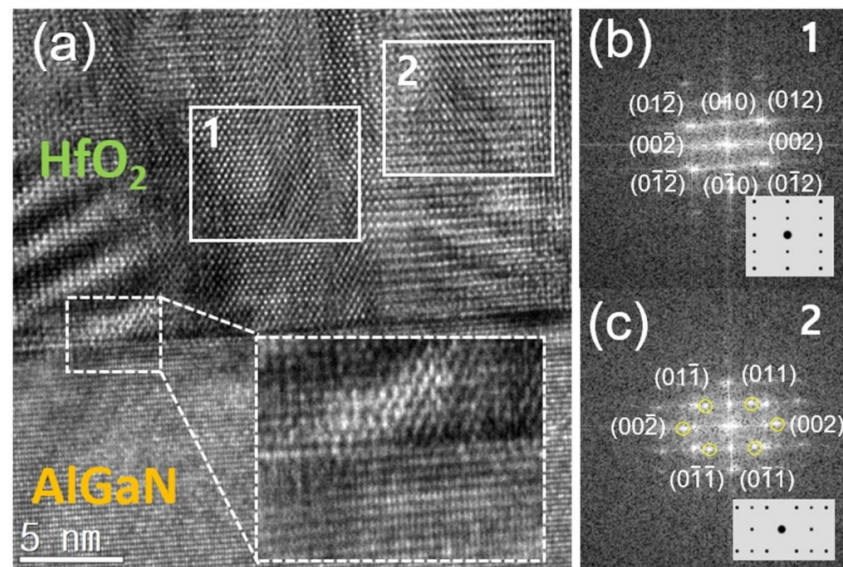


Figure 2. (a) A cross-sectional HR-TEM image of the HfO₂/AlGaIn with the inset showing the magnified image at the interface region. TEM diffraction patterns (zone axis = [100]) from the regions (b) 1 and (c) 2 with the insets showing the simulated diffractions patterns of the orthorhombic (Pca₂) and tetragonal (P42/nmc) phased for regions 1 and 2, respectively.

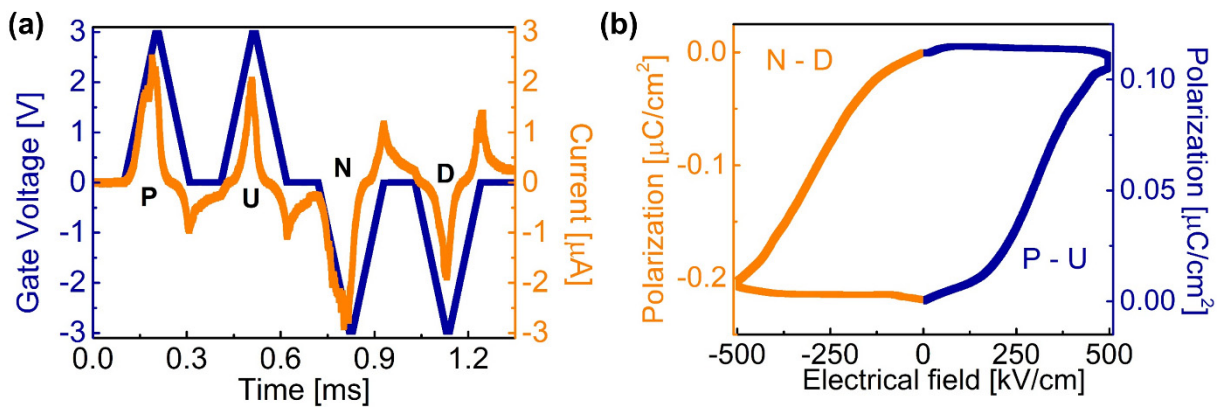


Figure 3. (a) PUND measurements using +3 V gate voltage pulses on the fabricated AlGaIn MOSCAP. (b) Gate voltage-dependent polarization with the orange line from the N-D half polarization curve and navy line from P-U half polarization curve.

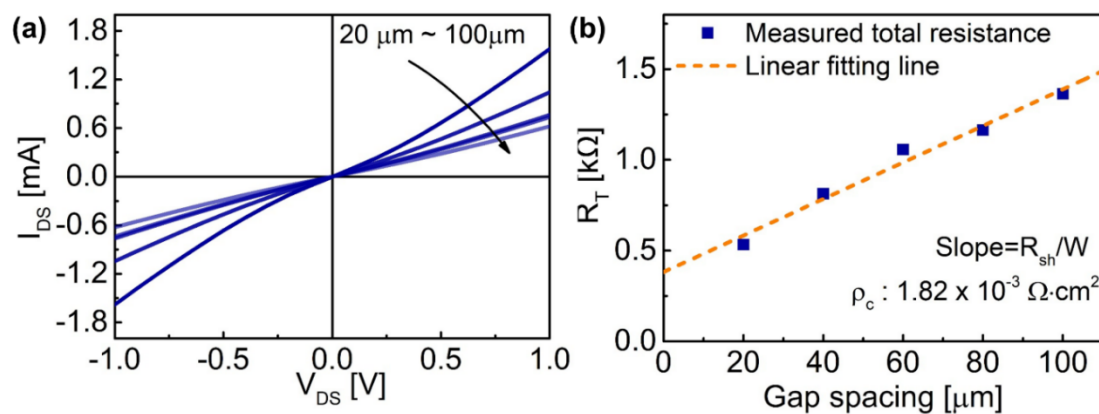


Figure 4. (a) The I_{DS} vs. V_{DS} curve measured at TLM pattern with different gap spacing from 20 μm to 100 μm . (b) The total resistance and contact resistivity which were calculated from Figure 2a.

To examine the ferroelectricity of the HfO₂ layer, the P-V PUND measurements were performed on the fabricated HfO₂/AlGa_N MOSCAP. PUND is a method that utilizes the displacement current (D) produced across a ferroelectric film. Before applying the positive switching voltage, D equals $2P_S + \epsilon E$, where P_S is a spontaneous polarization field, ϵ is a dielectric constant of an insulator, and E is an applied field. The second positive pulse is a non-switching pulse that makes D simply ϵE . Therefore, the spontaneous polarization charge induced by a ferroelectric film is given by the difference in D between the first and second pulses. When it comes to measuring the actual polarization charge in a MOSCAP, a typical metal–insulator–metal (MIM) capacitor is not ideal. The measured polarization charge from a MIM is often different from the actual polarization charge in a real MOS device due to the surface potential of the semiconductor and trapped-charge induced screening of polarization. The leakage current can also be affected by the difference in the barrier height between a MOSCAP and MIM. Furthermore, the crystallinity of a ferroelectric film deposited on metal is different from the one deposited on the semiconductor. As the ferroelectric property is dependent on the domains, crystallinity plays a critical role in the magnitude of spontaneous polarization. Therefore, this work followed the method suggested in [24] to perform PUND on our MOSCAP [22–24]. Figure 3a shows the current (orange) measured in response to the PUND pulses; P and N voltage pulses correspond to switching polarization. The measured current for N and D pulses is larger than that of P and U, which leads to different magnitudes for each polarization half-loop as calculated in Figure 3b. Moreover, the amount of switched charge for the N pulse is larger compared with the P pulse; the estimated induced charge ranges from 0.11 to 0.22 $\mu\text{C}/\text{cm}^2$. Considering the amount of 2DEG is $\sim 1.3 \mu\text{C}/\text{cm}^2$ (carrier concentration = $7.9 \times 10^{12}/\text{cm}^2$), these additional charges induced by the polarization are expected to increase the carrier density of 2DEG by $\sim 10\%$ and thereby lower the subthreshold swing of HEMTs.

Figure 5 shows the electrical characteristics of a representative device with L_G of 10 μm , channel length (L_{DS}) of 30 μm , and channel width (W) of 100 μm . Figure 5a shows the transfer curves (I_{DS} – V_{GS}) normalized with W for $V_{DS} = 2$ and 10 V. The device exhibits a high on/off ratio of $>10^9$ and a negligible hysteresis (ΔV) related to the interfacial traps [25]. ΔV is approximately 160 and 70 mV at V_{DS} of 2 and 10 V, respectively. I_{DS} is lower than state-of-the-art devices due to the long channel length and unoptimized device structure. However, Figure 5b illustrates the subthreshold slope (SS) close to 60 mV/dec during the transient owing to the abrupt HfO₂ (with spike RTA)/Ga_N interface confirmed by TEM analyses. The SS of 73.6 and 58.9 mV/dec is calculated from

$$S = \frac{dV_{GS}}{d(\log_{10} I_{DS})} \quad (1)$$

under forward and backward V_{GS} sweeps, respectively, with 0.05 V/step and $V_{DS} = 2$ V. In addition to the TEM analysis in Figure 2 and small ΔV , the interface trap density (D_{it}) was estimated using the equation

$$D_{it} = \frac{C_i}{q^2} \left(\frac{qSS}{kT \ln 10} - 1 \right) \quad (2)$$

The obtained D_{it} of $8.64 \times 10^{11} \text{ eV}^{-1} \text{ cm}^{-2}$ is comparable to D_{it} of more conventional MOS-HEMTs such as the ones with Al₂O₃. Therefore, the spike-annealing process does not seem to degrade the interface. Considering the similar D_{it} and material quality of our devices to the others, the lower SS of our devices is likely to be related to the weak ferroelectricity of the undoped HfO₂ layer. Furthermore, note that even lower SS was observed during the backward sweep due to the ferroelectric dipoles within the HfO₂ aligned toward the direction of HEMTs dipoles [26]. Figure 5c shows negligible current crowding and therefore good ohmic contacts. At $V_{GS} = -3$ V, however, self-heating of the device led to the lowering of I_{DS} in the saturation region. As shown by Figure 5d, the off-state breakdown of the device ($L_{GD} = 10 \mu\text{m}$) occurs at V_{DS} of ~ 400 V with $V_{GS} = -9$ V.

The observed off-state I_{DS} was a few orders of magnitude higher than other measured I-V results in this work due to the high voltage measurement set-up.

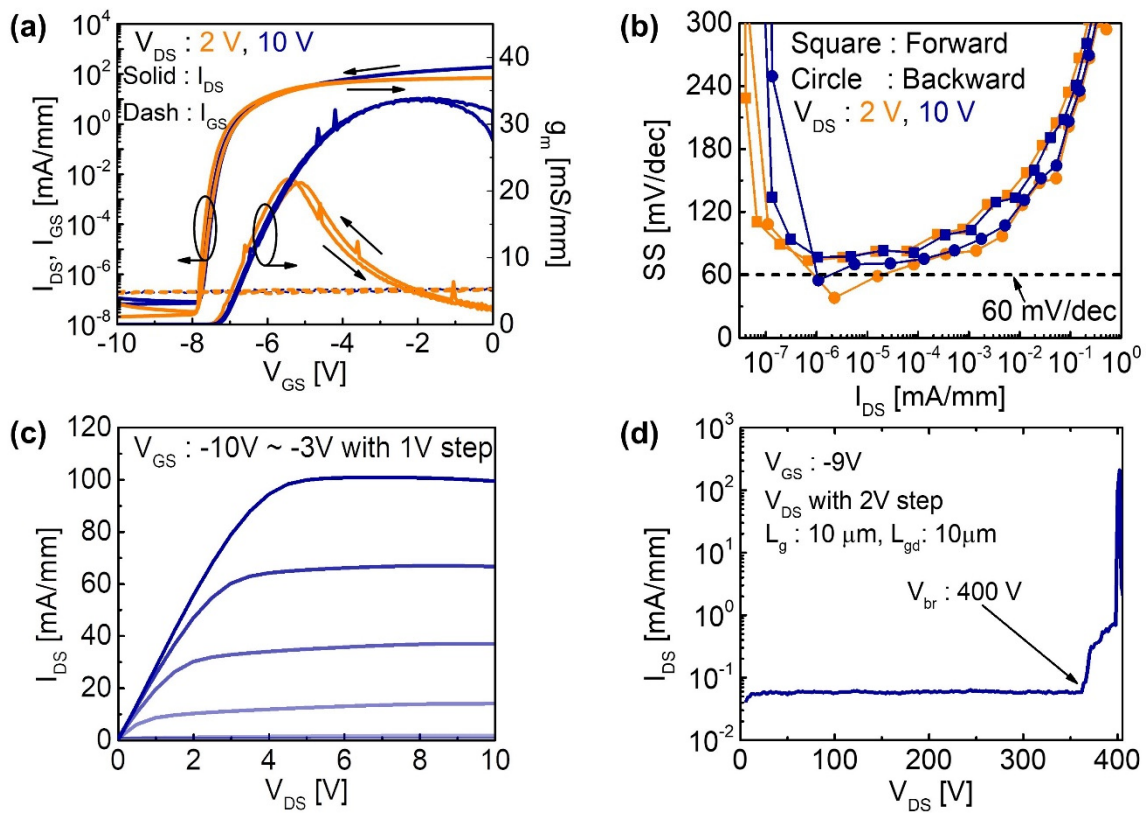


Figure 5. (a) I_{DS} - V_{GS} and transconductance curves with V_{DS} at 2 V (orange) and 10 V (navy). (b) Measured subthreshold slope as a function I_{DS} in forward (square) and backward (circle) directions with V_{DS} = 2 (orange) and 10 V (navy). (c) I_{DS} - V_{DS} curves at various V_{GS} . (d) Off-state showing breakdown at ~400 V.

Figure 6a shows the on/off ratio and SS values as a function of L_G . A high on/off ratio of $>10^9$ was maintained while exhibiting steep SS below 60 mV/dec under backward V_{GS} sweep. Figure 6b summarizes the reported SS and on/off ratio. Our MOS-HEMTs ($L_G = 10 \mu\text{m}$) show a relatively high on/off ratio of $>10^9$ with near-ideal SS of 60 mV/dec. This study strongly suggests the spike annealing of HfO_2 at 600 °C can induce ferroelectricity while maintaining the pristine HfO_2/GaN interface with low D_{it} .

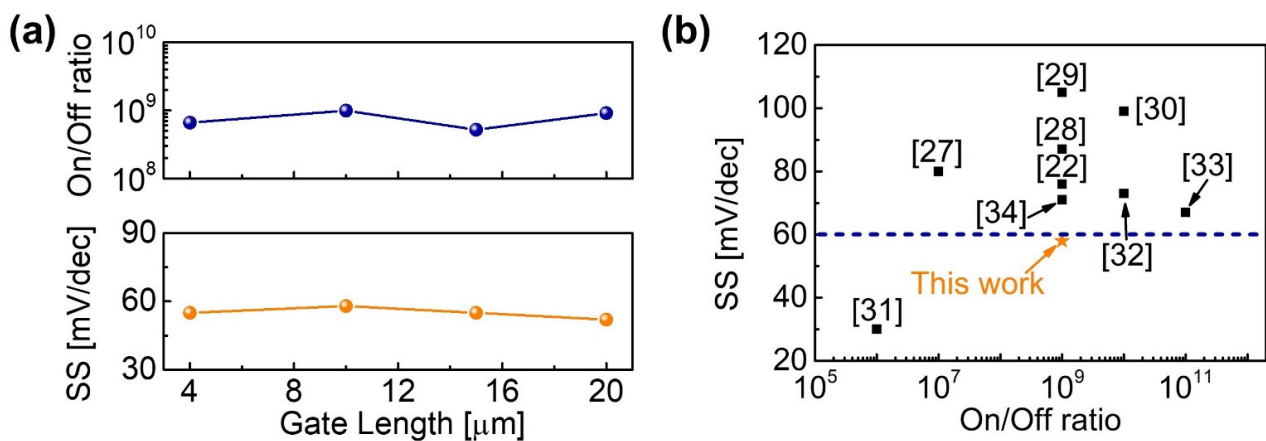


Figure 6. (a) Measured on/off ratio and SS as a function of the gate length. (b) Comparison of SS and on/off ratio values from various AlGaN/GaN MOS-HEMTs with a different gate dielectric as indicated.

4. Conclusions

In summary, we investigated the impact of undoped HfO₂-based ferroelectric gate dielectric on the device performance of AlGa_{0.5}N/GaN HEMTs. The spike annealing process at 600 °C induced the orthorhombic phase, which is likely the origin of observed ferroelectric behavior. TEM analysis confirmed the atomically abrupt HfO₂/nitride interface with no interlayer and an overall D_{it} of $8.64 \times 10^{11} \text{ eV}^{-1} \text{ cm}^{-2}$ was estimated from the SS. The combination of the enhanced ferroelectricity and high interfacial quality led to SS close to 60 mV/dec and on/off ratio $>10^9$. These results show that the HfO₂-based ferroelectric gate can improve the efficiency of AlGa_{0.5}N/GaN MOS-HEMTs without compromising the overall performance of HEMTs.

Author Contributions: Conceptualization: G.Y., M.J.Y. and J.Y.Y.; methodology: M.J.Y., J.Y.Y. and J.H.; formal analysis: M.J.Y., J.Y.Y. and C.H.L.; investigation: all authors; writing—original draft preparation: M.J.Y. and J.Y.Y.; writing—review and editing: G.Y. and R.B.K.C.; visualization: M.J.Y. and J.Y.Y.; supervision: G.Y. and R.B.K.C.; funding acquisition: G.Y. and R.B.K.C. All authors have read and agreed to the published version of the manuscript.

Funding: This work was supported by the national R&D Program through the National Research Foundation of Korea (NRF) funded by the Ministry of Science and ICT (2021R1A4A1033155, 2021R1F1-A1058006) and NRF funded by the Ministry of Education (grant no. NRF-2021R111A3054907).

Data Availability Statement: The data presented in this study are available on request from the corresponding author.

Acknowledgments: The EDA tool was supported by the IC Design Education Center, Korea.

Conflicts of Interest: The authors declare no conflict of interest. The funders had no role in the design of the study; in the collection, analyses, or interpretation of data; in the writing of the manuscript; or in the decision to publish the results.

References

- Chen, K.J.; Häberlen, O.; Lidow, A.; Tsai, C.L.; Ueda, T.; Uemoto, Y.; Wu, Y. GaN-on-Si Power Technology. *IEEE Trans. Electron Devices* **2017**, *64*, 779–795. [[CrossRef](#)]
- Amano, H.; Baines, Y.; Beam, E.; Borga, M.; Bouchet, T.; Chalker, P.R.; Charles, M.; Chen, K.J.; Chowdhury, N.; Chu, R.; et al. The 2018 GaN power electronics roadmap. *IOPsci. J. Phys. D Appl. Phys.* **2018**, *51*, 163001. [[CrossRef](#)]
- Ghosh, S.; Ahsan, S.A.; Dasgupta, A.; Khandelwal, S.; Chauhan, Y.S. GaN HEMT modeling for power and RF applications using ASM-HEMT. In Proceedings of the 2016 3rd International Conference on Emerging Electronics (ICEE), Mumbai, India, 27–30 December 2016; pp. 1–3.
- Zanoni, E.; Meneghini, M.; Meneghesso, G.; Bisi, D.; Rossetto, I.; Stocco, A. Reliability and failure physics of GaN HEMT, MIS-HEMT and p-gate HEMTs for power switching applications: Parasitic effects and degradation due to deep level effects and time-dependent breakdown phenomena. In Proceedings of the 2015 IEEE 3rd Workshop on Wide Bandgap Power Devices and Applications (WiPDA), Blacksburg, VA, USA, 2–4 November 2015; pp. 75–80.
- An, D.; Lee, B.H.; Lim, B.O.; Lee, M.K.; Kim, S.C.; Oh, J.H.; Kim, S.D.; Park, H.M.; Shin, D.H.; Rhee, J.K. High switching performance 0.1- μm metamorphic HEMTs for low conversion loss 94-GHz resistive mixers. *IEEE Electron Device Lett.* **2005**, *26*, 707–709.
- Ando, Y.; Kaneki, S.; Hashizume, T. Improved operation stability of Al₂O₃/AlGa_{0.5}N/GaN MOS high-electron-mobility transistors grown on GaN substrates. *Appl. Phys. Express* **2019**, *12*, 024002. [[CrossRef](#)]
- Shi, Y.T.; Lu, H.; Xu, W.Z.; Zeng, C.K.; Ren, F.F.; Ye, J.D.; Zhou, D.; Chen, D.J.; Zhang, R.; Zheng, Y. High-k HfO₂-Based AlGa_{0.5}N/GaN MIS-HEMTs with Y₂O₃ Interfacial Layer for High Gate Controllability and Interface Quality. *IEEE J. Electron Devices Soc.* **2020**, *8*, 15–19. [[CrossRef](#)]
- Fontserè, A.; Pérez-Tomás, A.; Godignon, P.; Millán, J.; De Vleeschouwer, H.; Parsey, J.M.; Moens, P. Wafer scale and reliability investigation of thin HfO₂-AlGa_{0.5}N/GaN MIS-HEMTs. *Microelectron. Reliab.* **2012**, *52*, 2220–2223. [[CrossRef](#)]
- Park, M.H.; Lee, Y.H.; Hwang, C.S. Understanding ferroelectric phase formation in doped HfO₂ thin films based on classical nucleation theory. *Nanoscale* **2019**, *11*, 19477–19487. [[CrossRef](#)] [[PubMed](#)]
- Kobayashi, M.; Hiramoto, T. On device design for steep-slope negative-capacitance field-effect-transistor operating at sub-0.2V supply voltage with ferroelectric HfO₂ thin film. *AIP Adv.* **2016**, *6*, 025113.
- Tokumitsu, E. Oxide-Channel Ferroelectric-Gate Thin-Film Transistors with Nonvolatile Memory Function. *Top. Appl. Phys.* **2020**, *131*, 111–124.
- Wu, C.; Ye, H.; Shaju, N.; Smith, J.; Grisafe, B.; Datta, S.; Fay, P. Hf_{0.5}Zr_{0.5}O₂-Based Ferroelectric Gate HEMTs with Large Threshold Voltage Tuning Range. *IEEE Electron Device Lett.* **2020**, *41*, 337–340. [[CrossRef](#)]

13. Chang, Y.C.; Huang, M.L.; Chang, Y.H.; Lee, Y.J.; Chiu, H.C.; Kwo, J.; Hong, M. Atomic-layer-deposited Al₂O₃ and HfO₂ on GaN: A comparative study on interfaces and electrical characteristics. *Microelectron. Eng.* **2011**, *88*, 1207–1210. [[CrossRef](#)]
14. Gunawan, R.; Jung, M.Y.L.; Seebauer, E.G.; Braatz, R.D. Optimal control of rapid thermal annealing in a semiconductor process. *J. Process Control* **2004**, *14*, 423–430. [[CrossRef](#)]
15. Lee, C.H.; Yang, J.Y.; Heo, J.S.; Yoo, G.W. Graded Crystalline HfO₂ Gate Dielectric Layer for High-k/Ge MOS Gate Stack. *IEEE J. Electron Devices Soc.* **2021**, *9*, 295–299. [[CrossRef](#)]
16. Yang, J.Y.; Ma, J.Y.; Lee, C.H.; Yoo, G.W. Polycrystalline/Amorphous HfO₂ Bilayer Structure as a Gate Dielectric for β -Ga₂O₃ MOS Capacitors. *IEEE Trans. Electron Devices* **2021**, *68*, 1011–1015. [[CrossRef](#)]
17. Schroeder, U.; Yurchuk, E.; Müller, J.; Martin, D.; Schenk, T.; Polakowski, P.; Adelman, C.; Popovici, M.I.; Kalinin, S.V.; Mikolajick, T. Important of different dopants on the switching properties of ferroelectric hafnium oxide. *IOPsci. J. Phys. D Appl. Phys.* **2014**, *53*, 08LE02.
18. Sang, X.; Grimley, E.D.; Schenk, T.; Schroeder, U.; Lebeau, J.M. On the structural origins of ferroelectricity in HfO₂ thin films. *Appl. Phys. Lett.* **2015**, *106*, 162905. [[CrossRef](#)]
19. Polakowski, P.; Müller, J. Ferroelectricity in undoped hafnium oxide. *Appl. Phys. Lett.* **2015**, *106*, 232905. [[CrossRef](#)]
20. Nishimura, T.; Xu, L.; Shibayama, S.; Yajima, T.; Migita, S.; Toriumi, A. Ferroelectricity of nondoped thin HfO₂ films in TiN/HfO₂/TiN stacks. *IOPsci. J. Phys. D Appl. Phys.* **2016**, *55*, 08PB01.
21. Schroder, D.K. *Semiconductor Material and Device Characterization*; Wiley-IEEE Press: New York, NY, USA, 2006; Volume 3.
22. Que, T.T.; Zhao, Y.W.; Qiu, Q.L.; Li, L.A.; He, L.; Zhang, J.W.; Feng, C.L.; Liu, Z.X.; Wu, Q.S.; Chen, J. Evaluation of stress voltage on off-state time-dependent breakdown for GaN MIS-HEMT with SiN_x gate dielectric. *Chin. Phys. B* **2020**, *29*, 107201. [[CrossRef](#)]
23. Scott, J.F.; Kammerdiner, L.; Parris, M.; Traynor, S.; Ottenbacher, V.; Shawabkeh, A.; Oliver, W.F. Switching kinetics of lead zirconate titanate submicron thin-film memories. *J. Appl. Phys.* **1988**, *64*, 787–792. [[CrossRef](#)]
24. Moghadam, R.M.; Xiao, Z.; Ahmadi-Majlan, K.; Grimley, E.D.; Bowden, M.; Ong, P.V.; Chambers, S.A.; Lebeau, J.M.; Hong, X.; Sushko, P.V.; et al. An Ultrathin Single Crystalline Relaxor Ferroelectric Integrated on a High Mobility Semiconductor. *Nano Lett.* **2017**, *17*, 6248–6257. [[CrossRef](#)] [[PubMed](#)]
25. Shen, J.; Zhang, C.Y.; Xu, T.T.; Jiang, A.N.; Zhang, Z.Y.; Wang, S.; Chen, Q. Hysteresis-free HfO₂ film grown by atomic layer deposition at low temperature. *Thin Solid Films* **2011**, *519*, 7723–7726. [[CrossRef](#)]
26. Zhang, M.; Kong, Y.; Zhou, J.; Xue, F.; Li, L.; Jiang, W.; Hao, L.; Luo, W.; Zeng, H. Polarization and interface charge coupling in ferroelectric/AlGaIn/GaN heterostructure. *Appl. Phys. Lett.* **2012**, *100*, 112902. [[CrossRef](#)]